Journal Name

ARTICLE

Versatile Iron-Catechol based Nanoscale Coordination Polymers. Antiretroviral Ligand Functionalization and their use as Efficient Carriers in HIV/AIDS Therapy

Received 00th January 20xx,
Accepted 00th January 20xx

DOI: 10.1039/x0xx00000x

Rubén Solórzano[a,b],Olivia Tort[c], Javier García-Pardo[a], Tuixent Escribà[c], Julia Lorenzo[d], Mireia Arnedo[c], Daniel Ruiz-Molina[a], Ramon Alibés[b], Félix Busqué*[b] Fernando Novio*[a]

A novel chemical approach integrating the benefits of nanoparticles with the versatility of coordination chemistry is reported here to increase the effectiveness of well-known HIV antiretroviral drugs. The novelty of our approach is illustrated using a catechol ligand tethered to the known antiretroviral AZT as a consitutive building block of the nanoparticles. The resulting nanoscale coordination polymers ensure good encapsulation yields and equivalent antiretroviral activity while significantly diminishing its cytotoxicity. Moreover, this novel family of nanoparticles also offer: i) long lasting drug release dissimilar inside and outside the cells depending on pH, ii) triggering in the presence of esterases, activating in an on-off manner the antiviral activity, thanks to a proper chemical design of the ligand and iii) improved colloidal stabilities and cellular uptakes (up to 50 fold increase). The presence of the iron nodes also adds multifunctionality as possible contrast agents. The present study demonstrates the suitability of NCPs bearing pharmacologically active ligands as an alternative to conventional antiretroviral treatments.

Introduction

The lifelong treatment of Human Immunodeficiency Virus (HIV) infection nowadays still faces several drawbacks: 1) daily dosing can be cumbersome for the patient; 2) the existence of cellular reservoirs of latent HIV viruses that escape the treatment;[1-4] 3) limited capacity of antiretroviral (ARV) drugs to access tissue reservoirs and sanctuaries i.e. central nervous system, lymph nodes or lungs;[5] 4) low solubility and poor bioavailability of the antiviral drugs; and 5) drug resistance development after continued treatment and the corresponding side effects.[6,7] With no definitive cure and forced to suffer these long-life side effects, the target for HIV drug administration has concentrated on decreasing long-term toxicity and the development of new treatment strategies that do not rely on daily medication through the development of new nanoscopic platforms for drug delivery.[8-13] Nanocarriers can also facilitate drug transport and entrance to all infected $CD4^+$ cells reservoirs throughout the body, present even in patients who have had undetectable HIV RNA plasma levels for years,[14] facilitating its elimination.

So far, different combinations of nanostructured ARV drugs have been reported using protein-based lactoferrin,[15] polymeric nanoparticles[16-18] or lipids.[19,20] In most of these examples modest to low drug loading contents, usually oscillating around 5 wt%, are achieved. More effective encapsulation processes have been shown on nanoscale metal-organic frameworks (nano-MOFs)[21-24] with antiretroviral drug loadings up to 42 wt%[23,25] or in drug solid nanoparticles (up 70 wt%), obtained using emulsion-templated freeze-drying.[26,27] However, and in spite of these pioneering results, questions such as minimization of side effects, biodistribution improvement or the development of novel formulation allowing for the metabolization into a pharmacologically active drug, mainly intracellularly, still represents a real challenge. Therefore, the development of novel nanoformulations has become a foremost objective in HIV therapy.

Nanoscale coordination polymer particles (NCPs) embody a novel family of hybrid nanoparticles combining metal ions and organic ligands that can use drugs as constitutive building

[a] Catalan Institute of Nanoscience and Nanotechnology (ICN2), CSIC and BIST, Campus UAB, Bellaterra, 08193 Barcelona, Spain. E-mail: fernando.novio@icn2.cat
[b] Departament de Química, Universitat Autònoma de Barcelona (UAB), Campus UAB. Cerdanyola del Vallès 08193, Barcelona, Spain.
[c] Laboratory of Retrovirology and Viral Immunopathogenesis, Institut d'Investigacions Biomèdiques August Pi i Sunyer (IDIBAPS), 08036 Barcelona, Spain.
[d] Institut de Biotecnologia i de Biomedicina and Departament de Bioquímica i Biologia Molecular. Universitat Autónoma de Barcelona, 08193 Bellaterra, Barcelona, Spain.

Electronic Supplementary Information (ESI) available: [details of any supplementary information available should be included here]. See DOI: 10.1039/x0xx00000x

blocks (chemical entrapment),[28-31] though physical encapsulation has also been reported.[32-34] Chemical entrapment allows for a better fine-tuning of the release kinetics (up to many hours) as well as better formulation with increased encapsulation yields.[35] The use of active metal drugs, such as Pt(IV), as polymeric nodes of coordination polymers is the most representative and successful example of chemical entrapment.[29,36-38] Less explored has been the chemical entrapment through tethering of active drugs as chelating ligands, in spite of the fact that its efficiency has already been reported.[39] Moreover, the chemical flexibility of organic synthesis may allow for the design of drugs (ligands) cleaved under physiological conditions.[40]

As a model compound for these studies, we have selected the broadly studied ARV drug azidothymidine (AZT) that selectively inhibits the HIV-1 reverse transcriptase (Fig. 1a). AZT was long used in the past as an effective antiretroviral drug that rapidly metabolized in the liver to the inactive glucoronide form resulting in poor bioavailability with high residual toxic effects when administered orally.[41] Therefore, this antiretroviral drug represents an adequate example to validate our approach. Specifically we proposed the functionalization of AZT at the 5´-OH position with a chelating catechol group (catAZT, see Fig. 1a). Functionalization at this position has already been shown to be successful for the synthesis of AZT prodrugs with chemical and/or enzymatic hydrolysis.[42,43] Afterwards, this ligand, in combination with an iron salt and a bisdentate ligand is used to form the nanoparticles (see Fig 1a). Finally, the release of the drug is expected to take part following a two-step mechanism: I) liberation of the catAZT from the nanoparticle in a pH controlled process and second, liberation of the free AZT drug from the catechol unit in the presence of the corresponding enzymes (see Fig. 1b). For comparison purposes, to test possible effects of the material without containing an antiretroviral drug, the use of the analogous but inactive thymidine (THY) is also proposed (see Fig. 1a).

Results and discussion

Synthesis and characterization of catAZT and catTHY

The synthesis of catAZT was achieved through a 5-step synthetic sequence in 32% overall yield starting from commercially available 3,4-dibenzyloxybenzaldehyde (see Fig. 2a and ESI S1† for details) which reacted with 4-carboxybutyltriphenylphosphonium bromide and sodium hydride in dry toluene to afford the olefin **2** in 88% yield as a 5:1 mixture of the *Z* and *E* isomers. The use of other bases and solvents, such as potassium *tert*-butoxide in dry THF proved to be less efficient for this process. Simultaneous hydrogenation of the alkene moiety and removal of the benzyl protecting group, at high pressure of H_2 under Pd/C catalyst in EtOAc, leaded to catechol **3** in almost quantitative yield. Protection of the hydroxyl groups of **3** as their *tert*-butyldiphenylsilyl (TBDPS) derivatives was accomplished by using TBDPSCl and 1,8-diazabicyclo[5.4.0]undec-7-ene (DBU) in dry acetonitrile, affording common intermediate **4** in 64% yield. Next, the nucleoside analogue AZT was tethered to this compound using 1-[Bis(dimethylamino)methylene]-1*H*-1,2,3-triazolo[4,5b] pyridinium 3-oxid hexafluorophosphate (HATU) as a coupling reagent and *N,N*-Diisopropylethylamine (DIPEA) as base in THF

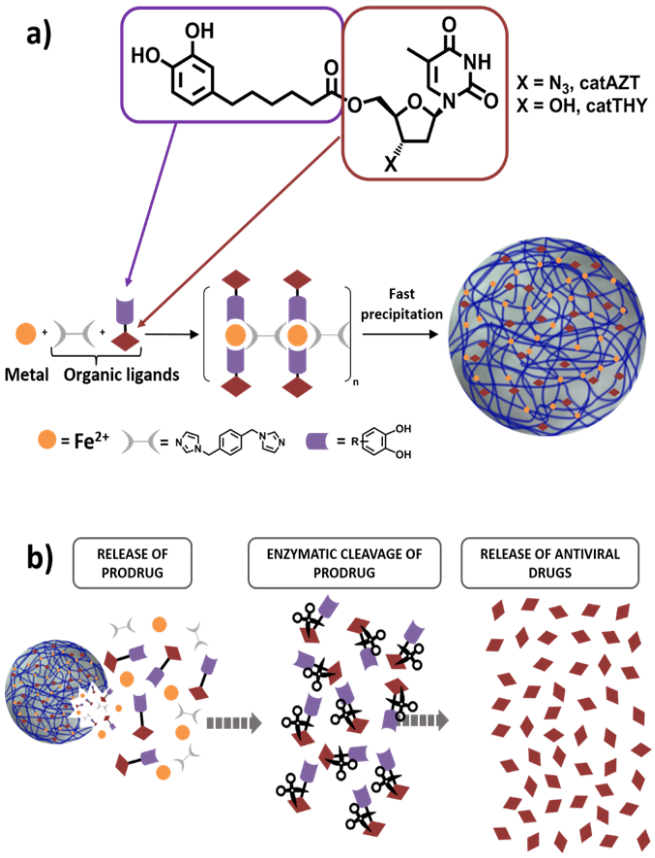

Fig. 1 (a) Schematic representation of a catechol ligand linked to the antiviral drug AZT by an enzymatically-cleavable bond via the carboxylic group. Posterior incorporation of catAZT or catTHY into a mixture containing iron and a bridging bis-imidazol ligand results in nanoparticle formation induced by fast precipitation of the coordination polymer formed. (b) Schematic representation of the antiviral release process, from the nanoparticles constructs to the AZT drug. It involves two main steps: I) release of the catAZT ligand most likely due to particle degradation and II) enzymatic cleavage of the free catechol derivative containing AZT.

leading to derivative **5** in 86% yield. Final removal of the protecting silyl groups of **5** was achieved by using triethylamine trihydrofluoride affording the target compound CatAZT in 68% yield. Synthesis of catTHY, changing azidothymidine by thymidine, was also faced from the common intermediate **4**. However, initial attempts to carry out the coupling reaction of **4** with thymidine using conventional coupling reagents (HATU, EDCl/HOBt or CDI) under standard conditions were unsuccessful. After some experimentation, it was found that the reaction of thymidine with **4** under Mitsunobu conditions (Ph_3P and DBAB) delivered the 5'-substituted compound **6** in 56% yield. After coupling, treatment with triethylamine trihydrofluoride removed the silyl protecting group to afford CatTHY in 68% yield (see Fig. 2a and ESI S1† for details).

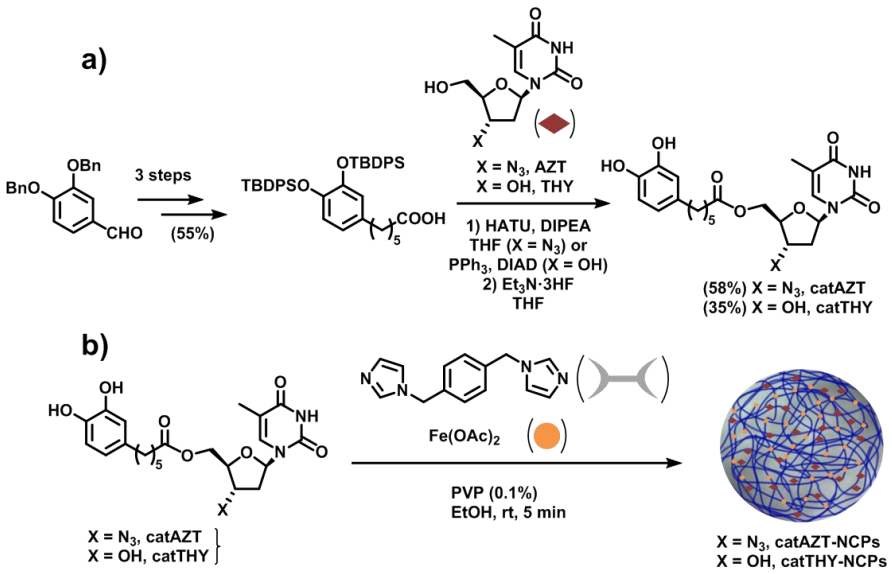

Fig. 2 (a) Schematic of catAZT and catTHY synthesis. (b) Preparation of catAZT and catTHY-containing nanoparticles.

Next experiments aimed to determine the kinetics of the enzymatic hydrolysis of catAZT in PBS/BSA 0.5 mM, 37 °C. As shown in Fig. 3, in the absence of pig liver esterase (PLE), and independently of the pH used, there was almost no hydrolysis of the ligand (ca. 35% in 72 h, pH 7.4). On the contrary, addition of PLE under the same experimental conditions resulted in a fast release of the antiviral drug (ca. 90% in 1 h). The release profile for both pH 5.1 and 7.4 offered similar results, indicating a weak dependence of the enzymatic activity to the pH.

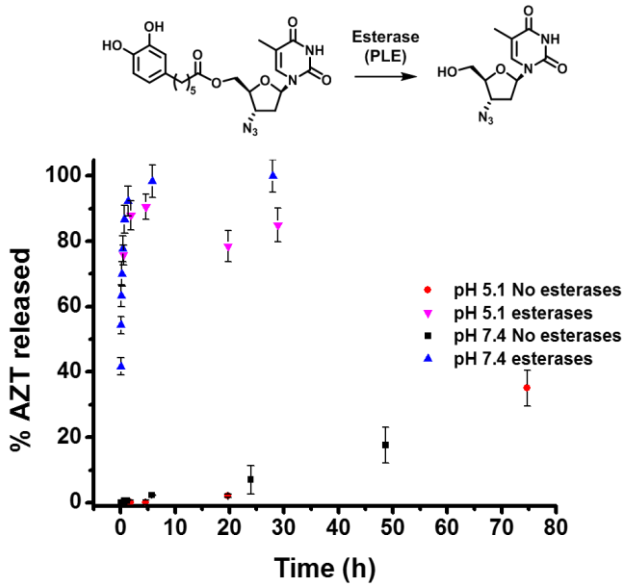

Fig. 3 Hydrolysis kinetics of catAZT in the absence (no esterases) or presence (esterases) of pig liver esterases (PLE) at the indicated pH values. In all cases, experiments were performed in a PBS/BSA 0.5 mM buffer at 37 °C. At the top, schematic representation of the enzymatic cleavage of catAZT by pig liver esterases (PLE).

Synthesis and characterization of the nanoparticles

Ligand catAZT was used to prepare the corresponding antiretroviral nanoparticles (ARV-NCP) catAZT-NCP following a well stablished methodology[32] consisting in the direct reaction of the catechol ligand and 1,4-bis(imidazol-1-ylmethyl)benzene (bix) with iron(II) acetate using polyvinylpyrrolidone (PVP) as stabilizing agent (Fig. 2b). After vigorous stirring at room temperature, a dark-purple precipitate was collected by centrifugation, washed several times with ethanol, and dried under vacuum. The synthetic procedure is detailed in the experimental section and complete nanoparticle characterization is summarised in Supplementary Information (see ESI S2†). SEM images revealed the formation of spherical catAZT-NCPs nanoparticles with an average diameter of 147±33 nm (Fig. 4a) while dynamic light scattering (DLS) studies showed an average hydrodynamic radius of 202 ± 10 nm (PDI = 0.07) in ethanol (see ESI S2†, Fig. S1).

The X-ray powder diffraction (XRD) pattern was characteristic of an amorphous material (see ESI S2†, Fig. S2). The Fourier-transform infrared (FTIR) spectra confirmed the coordination of the bix and prodrug ligands to the metal (see Fig. 4b). Characteristic bands for the asymmetric azido stretching band are observed at both catAZT (2108 cm^{-1}) and catAZT-NCPs (2106 cm^{-1}). Characteristic bands for Bix (1508, 1228 and 1103 cm^{-1}) are also observed at catAZT-NCPs FTIR spectrum (1519, 1263 and 1097 cm^{-1}, respectively). Finally, elemental analysis, NMR and ICP measurements data agreed with the presence of the different elements with a general chemical formula $[Fe(catAZT)_{1.5}(bix)_{0.6}(AcO)(H_2O)_{2.4}]$ (see ESI S2†, Table S1 and Fig. S3). The stoichiometric deviation from the theoretical results, quite common for NCPs, arises from the out-of-equilibrium conditions used for the synthesis of the nanoparticles. In any case, the reaction is really reproducible as shown by elemental analysis and a complete chemical characterization of at least three different and independent synthetic batches. HPLC quantification of the AZT prodrug showed a loading content of 25% in weight (44% of catAZT), in agreement with the expected value from the previous chemical formula (for detailed characterization see ESI S2†, Fig. S4-S5). ICP measurements for the iron metal ion (5.46%), were also in agreement with that deduced from the formula of elemental analysis (5.50%). Although the original source of iron is a Fe^{2+} salt, the complex was stabilized as high-spin Fe^{3+} as shown by Mössbauer spectroscopy (see ESI S2†, Fig. S6). This electronic modification results from a redox interplay between the metal ion and the electroactive catechol ligands in air as previously reported.[44]

Complementarily, model catTHY-NCPs nanoparticles were also synthesized and tested for comparison purposes. catTHY-NCPs nanoparticles showed comparable physicochemical features to those found for catAZT-NCPs , for example, an average diameter of 87± 26 nm was measured by SEM micrographs and an average hydrodynamic radius of 170±2 nm (PDI = 0.14) in ethanol by DLS. (for complete characterization see ESI S3†).

Colloidal stability. Zeta-potential values close to -8.0 mV were obtained for catAZT-NCPs dispersed in 20 mM PBS buffer at pH 7.4. In agreement with such low values, a time dependent aggregation process was observed that eventually ended up with the precipitation of the sample, even at low-moderate concentrations. The addition of Bovine Serum Albumin (BSA) has been extensively used for dispersing inorganic and polymeric nanoparticles.[45,46] In our case, fluorescence quenching studies of BSA in the presence of NCPs (see ESI S2†, Fig. S7) suggested an interaction of the NCPs with the surface of this model protein. Accordingly, in the presence of such protein nanoparticles turn out to be stable except at very high concentrations (i.e concentrations >2 mg/ml) where the addition of additional sucrose is needed (see ESI S2†, Fig. S8).[47]

Cell viability. Toxicity to lymphocytic function is one of the major considerations in the clinical applicability of novel antiviral compounds. Moreover, it has been extensively demonstrated that AZT is highly toxic to human lymphocytes[48]. Therefore, we have examined the cytotoxic effect of the catAZT-NCPs nanoparticles against endogenous human CD4+ T

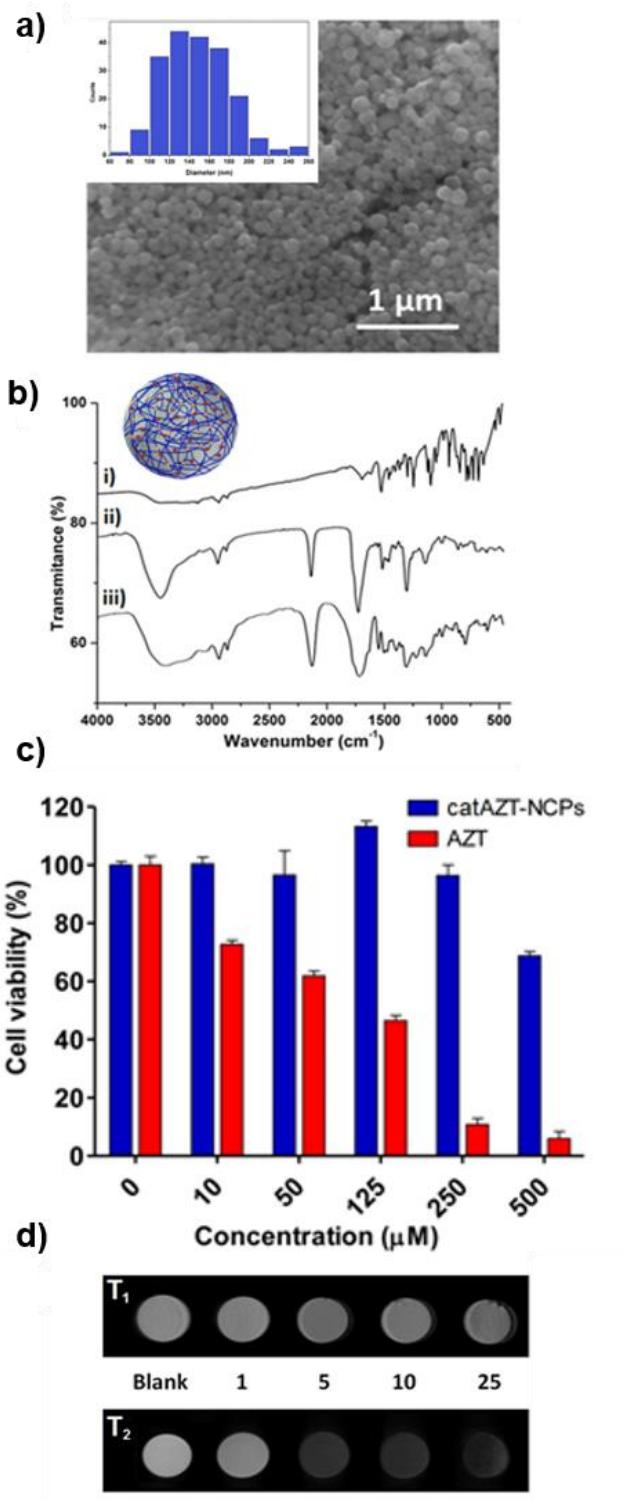

Fig. 4 (a) Representative SEM image of catAZT-NCPs. Inset: histogram of particle size extracted from SEM micrographs (200 particles, mean size 147 ± 33 nm. (b) FTIR spectra of i) Bix, ii) catAZT and iii) catAZT-NCPs. (c) Effect of catAZT-NCPs and free AZT on the cell viability of human primary CD4+ T lymphocytes. CD4+T cells were incubated during 24h in the presence of the indicated concentrations of catAZT-NCPs or AZT. Cell viability is expressed as percentage compared to an untreated control. Values are mean ± standard error of the mean (SEM) (n = 3). (d) ^{1}H MRI T1 and T2 phantoms maps of catAZT-NCPs in a PBS/agarose 1% solution at pH 7.4 at different concentrations (0, 1, 5, 10, 25 mM, referred to the Fe concentration).

lymphocytes. Primary CD4+ T cells were prepared by the rapid expansion method (REM) and treated for 24 h with catAZT-NCPs and free AZT, used as the reference compound (Fig. 4c). When the CD4+ T cells were treated with AZT, a clear cytotoxic effect was observed already at concentrations of 10 µM (or higher), with an IC50 value of 64 µM. To our surprise, when the same cells were treated with catAZT-NCPs, irrelevant cytotoxic effects were detected at least up to the highest concentration tested (500 µM). At this concentration, the nanoparticles maintained a cell viability of 70%, while for free AZT was <10% (IC50 > 500µM). These results confirmed that AZT remarkably reduced the toxicity on primary $CD4^+$ T lymphocytes upon nanostructuration.

MRI experiments. To confirm that the functionalization with AZT does not disrupt the multifunctional character of these nanoparticles, MR relaxometry experiments at different concentrations under an external magnetic field of 7 Teslas and in two phantom sequences, were done (Fig. 4d). The nanoprobes were dispersed in a PBS/agarose 1% to ensure a good colloidal stability. The obtained relaxation rate values were plotted versus the iron concentration reporting good linear correlations (see ESI S2†, Fig. S9). The iron-based NCPs exhibit a signal enhancement in a concentration-dependent manner and a T_1 positive contrast of r_1 = 0.15 mM^{-1} s^{-1}, and T_2 negative contrast of r_2 = 117.5 mM^{-1} s^{-1}. Curiously, these nanoparticles exhibit a low r_1 in comparison to the commonly used gadolinium contrast agents (i.e. Gd-DTPA; r_1= 3.3 $mM^{-1}s^{-1}$) or other related Iron-based NCPs (i.e. Fe-NCPs; (r_1=4.4 $mM^{-1}s^{-1}$).[49] However, they present a high T_2 negative contrast, which make these nanoparticles a very promising T_2 contrast agent with r_2 relaxivities nearly 25 times higher than Gd-DTPA.

Drug release profile

The release profile of AZT from the catAZT-NCP nanoparticles involves two main steps: 1) release of the catAZT ligand from the nanoparticles and 2) its transformation onto the active AZT prodrug upon enzymatic cleavage by esterases (see Fig. 5a). First experiments were done to determine the kinetics of catAZT release (step 1) by using HPLC for the quantification, upon incubation at 37 °C of the nanoparticles in a PBS/BSA 0.5 mM buffer solution at two different pHs, 5.1 and 7.4. First experiments in the absence of esterases at pH 7.4 showed no detectable presence of catAZT outside the dialysis bag, indicating the high stability of the coordination polymer at this pH (for more details see Experimental Section). Nevertheless, significant amounts were found at the lowest pH of 5.1, even at early stages of the release, due to the lower stability of the coordinative bond between the iron and the catechol at low pH values. This pH-triggered liberation of the catAZT ligand could favour the release inside the cells (i.e. acidic pH present in lysosomes), decreasing toxicity-associated side effects. Independently of the pH, and in the absence of esterases the presence of free AZT was low (≈ 15% at 72 h, see Figure 5b). Overall, the release rates are sufficient for the NCPs to circulate throughout the body at physiological pH enhancing its biodistribution.

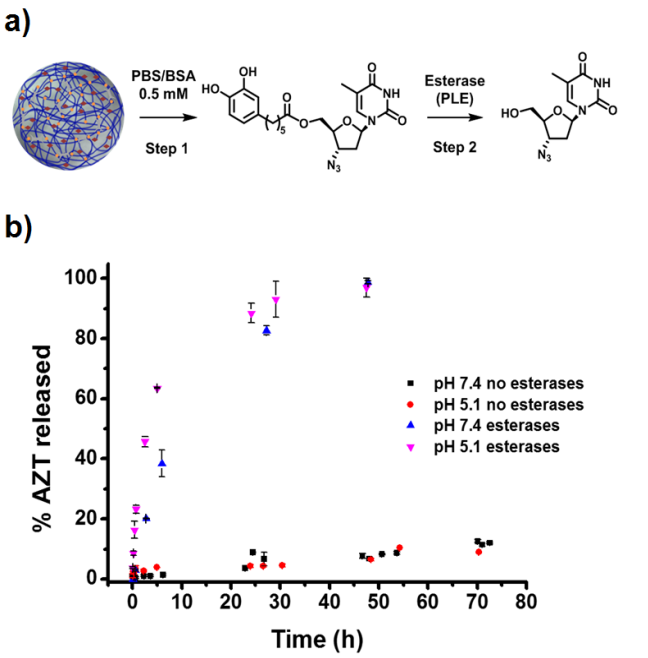

Fig. 5 (a) Schematic representation of the different release steps for the catAZT prodrug (step 1) and subsequent release of AZT (step 2). (b) AZT release kinetics from catAZT-NCPs in the absence (no esterases) or in the presence (esterases) of pig liver esterase (PLE) at pH 5.1 or 7.4. In all the cases, the experiments were performed in PBS/BSA buffer at 37 ºC (see experimental section for details).

Completely different results were obtained in the presence of the model esterase PLE (180 U/L). In this case, AZT release appeared to be faster, reaching almost up to 100% after 50 hours and with estimated half-lives of ~4.5 h (pH 5.1) and ~10 h (pH 7.4). These results confirmed that the enzymatic hydrolysis was fast, as previously described for the free catAZT ligand, so the limiting step was the release of the catAZT from the nanoparticles.

HIV-Antiviral activity of catAZT-NCPs

The antiviral activity of the whole set of synthesized nanoparticles and control molecules was tested on a model MT-2 human lymphocytic cell line by means of the MTT assay in a biohazard P3 laboratory specially prepared for it (for more info see Experimental Section). MT-2 cells is an established cell line of CD4+ T cells, easier to manipulate and obtain than primary human cells, thus suitable for first line studies of anti-HIV effect and, therefore broadly used to test the efficacy experimental antiviral agents thanks to its high reproducibility.[50-52] HIV-1 exerts a profound cytopathic (CPE) effect against CD4+ T lymphocytes. Once infected, the lymphocytes accumulate viral DNA and actively produce HIV proteins, which results in the concomitant lysis of such infected cells by apoptosis. MT-2 cells are profoundly sensitive to the CPE effect of HIV-1.

Uptake experiments. The therapeutic efficacy of an HIV-1 inhibitor depends on its intracellular concentration, which in turn is directly related with its uptake kinetics (in addition to other factors such as its metabolism and/or cellular efflux).[53, 54] To assess this question, MT-2 cells were incubated for 4 hours in the presence of different concentrations of catAZT-NCPs (AZT and catAZT were also used as model compounds). After this time, the amount of intracellular AZT was determined by HPLC-UV using an optimized procedure (see ESI S4† and Experimental Section for more details). The results shown in Fig. 6 indicate intracellular levels of AZT after direct exposure of the MT-2 cells to AZT, catAZT and catAZT-NCPs. The intracellular concentration of AZT up to concentrations of 500 µM (<0.070 nmols/10^6 cells) was undetectable after AZT or catAZT incubation. Only at extremely and unrealistic high concentration of such compounds of 1000 µM (see Fig. 6), detectable intracellular levels of AZT (0.81 ± 0.15 and 0.62 ± 0.11 nmols/10^6 for AZT and catAZT, respectively), were measured. Interestingly, concentrations of the catAZT-NCPs as low as 100 µM (normalized versus the AZT concentration) already resulted in detectable intracellular levels of AZT, with a significant concentration-dependent increase up to 500 µM (3.48 ± 0.33 nmols of AZT/10^6 cells).

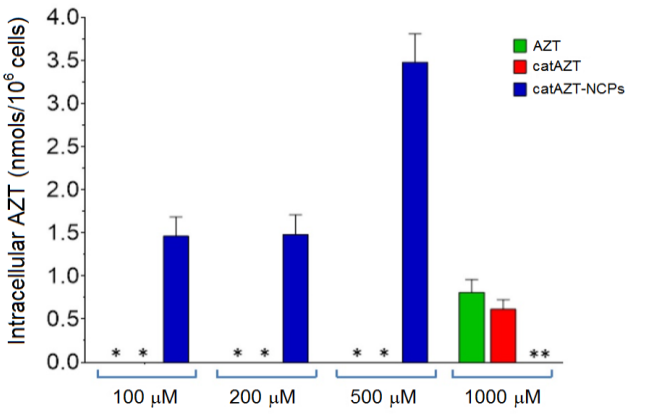

Fig. 6 Intracellular levels of AZT in MT-2 cells after 4h of incubation in the presence of different concentrations (100 µM, 200 µM, 500 µM, referred to the AZT equivalent concentrations) of AZT, catAZT or catAZT-NCPs. The asterisk (*) indicates those conditions with levels of AZT in the samples under the limit of detection of the method (<0.070 nmols/10^6 cells). For AZT and catAZT, an additional concentration of 1000 µM was assayed. Note that this concentration was not assayed for catAZT-NCPs (**) because nanoparticles were not stable at concentrations higher than 10 mg/ml.

Considering the detection limit of the HPLC method used for the quantification as a reference (<0.070 nmols/10^6 cells), we can easily estimate that treatment with the nanostructured material resulted in a >50 fold increase at 500 µM in comparison with free AZT. This could potentially be due to the mechanism of uptake. Nanoparticles are generally taken up by endocytosis mechanisms,[55-58] as opposed to small molecules, which are taken up by other different pathways. In the case of AZT, it has been described that enters inside the cell through membranes via passive diffusion and/or by uptake transporters.[59,60] Similar results were observed in a recent report, in which the nanoformulation of the antiviral drug dolutegravir resulted in higher uptake by human monocyte-derived macrophages in comparison with the free molecule.[61] It is worth to mention that cellular dolutegravir levels reached a maximum at 4 h after treatment with 100 µM of the nanoformulated drug.

HIV-Antiviral activity. The cytotoxicity on non-infected human MT-2 lymphocytes was at first determined. No appreciable cytotoxicity was observed for any of the antiretroviral agents at concentrations of 20 µM or lower after 3 or 7 days incubation except for the highest concentrations of the prodrug/ligand catAZT (100 µM), which showed reduced cell viability of ~70 % (for more info see ESI S5†, Fig. S18). When the same experiments were now repeated using MT-2 cells infected with the virus, a decrease of the cytopathic effect of HIV on human MT-2 cells was observed in the cultures treated with AZT, catAZT and catAZT-NCPs for 3 and 7 days treatment (see Fig. 7). In particular, a substantial increase in the cell viability was observed after three days following the order AZT > catAZT-NCPs > catAZT. Certainly, the most efficient antiviral

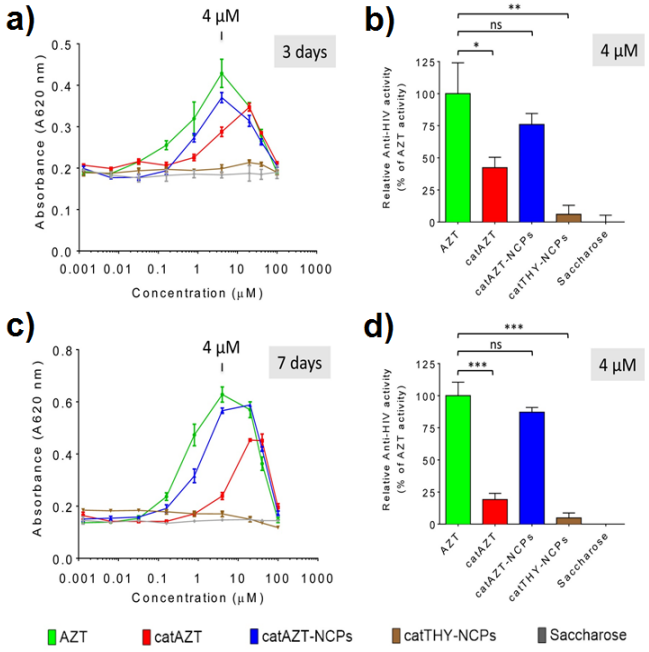

Fig. 7 HIV-antiviral activity. Cell viability of different concentrations of AZT, catAZT, catAZT-NCPs, and catTHY-NCPs on HIV-infected MT-2 cell culture after 3 days (a,b), and 7 days incubation (c,d) . The cytopathic effect of HIV (decrease in cell viability) is observed after incubating HIV-infected MT-2 cells with the compounds with no antiviral effect (catTHY-NCPs and saccharose). The antiviral effect of the compounds was indirectly measured as an increase in cell viability (increase in absorbance at 620 nm), as shown when incubating HIV-infected MT-2 cells in the presence of AZT, catAZT-NCPs or catAZT (a,c). (b,d) Relative Anti-HIV activity expressed as percentage compared to the absence of activity (saccharose) and maximal anti-viral activity in the assay determined for the most effective concentration of AZT (4 µM) after b) 3 days or d) 7 days incubation. An unpaired t-test was performed to compare anti-HIV efficacies of the compounds at 4 µM compared to the reference compound AZT. Note that the anti-viral efficacy of catAZT-NCPs was similar to that of AZT, while the effect of the prodrug catAZT and the control catTHY-NCPs were significantly lower. ns, non-significant; * p< 0.05; ** p< 0.01; *** p<0.0001.

response was obtained for the free AZT (followed closed by with the catAZT-NCPs), which recovered the cell viability within the 0.16-40 μM concentration range and with a maximum antiviral activity centered at 4 μM. At this concentration, the efficiency of catAZT-NCPs nanoparticles was slightly -but non-significantly- inferior than AZT, while the ligand catAZT showed the lowest activity (Fig. 7a and 7b). Control systems (i.e. catTHY-NCPs and saccharose) did not show any significant effect. Interestingly, when the same experiment was evaluated after seven days of incubation, the relative activity of AZT and catAZT-NCPs becomes now very similar (Fig. 7c), fact attributed to the accumulated long lasting release effect of the nanoparticles, while the difference of activity with catAZT ligand becomes more evident (Fig. 7d).

Conclusions

We have designed and synthesized novel iron-catechol based nanoscale coordination polymeric particles that incorporate a prodrug molecule tethered to a catechol ligand. To illustrate the potential of this nanoplatform we have used as catechol ligand (catAZT) a catechol linked, through an enzymatically cleavable ester bond, to the well-known antiretroviral AZT. The presence of a chelating catechol group allowed for the reproducible incorporation of catAZT with high payloads within coordination polymer nanoparticles of 147±5 nm average size. Following this approach, we have successfully reproduced the effective antiretroviral activity of the free AZT prodrug while the nanostructuration allows for the following significant advantages: I) stabilization of the drug in physiological media as a colloidal suspension; II) control over the release properties of the drug by the pH and the presence of enzymes, III) the nanoparticles retain the inherent multifunctionality thanks to the presence of iron ions with MRI responses, IV) significant reduction of the AZT toxicity and V) enhancement of the cellular uptake (up to 50 fold increase). catAZT-NCPs performed well its anti-HIV activity in cell assays, to equivalent levels than free AZT but over longer periods of time.

According with the previous results, the tethering of active drugs as coordinating ligands represent a novel but promising family of carriers to optimize the pharmacological characteristics of known antiretrovirals with a controlled release, while substantially minimizing side effects derived from systemic toxicity effects. Ongoing work is nowadays being developed to extend this novel approach to other diseases facing related challenges. It is expected that these new class of nanocarriers have the capacity to address challenges associated with delivering drug combinations, increasing bioavailability in tissue sanctuaries and latently infected cells, and improving cellular uptake; contributing to the development of the next generation of pharmacological strategies for HIV treatment.

Conflicts of interest

The authors declare no conflicts of interest.

Acknowledgements

This work was supported by project MAT2015-70615-R, MAT2012-35324, CTQ2013-44161-R, CTQ2016-75363-R and BIO2016-78057-R from the Spanish Government and FEDER funds. Authors also thank Instituto de Salud Carlos III (ISCIII), Madrid, Spain - Red de Investigación en SIDA (RIS), ISCIII-RETIC (RD16/0025/0002). R.S. thanks the Ministerio de Educación, Cultura y Deporte for the predoctoral grant FPU14/03170. The ICN2 is funded by the CERCA programme/Generalitat de Catalunya and supported by the Severo Ochoa programme of the Spanish Ministry of Economy, Industry and Competitiveness (MINECO, grant no. SEV-2013-0295). MR studies were carried out at the joint NMR facility of UAB and CIBER-BBN, Unit 25 of NANBIOSIS, with a 7T horizontal.

Notes and references

‡ Footnotes relating to the main text should appear here. These might include comments relevant to but not central to the matter under discussion, limited experimental and spectral data, and crystallographic data.

§

1. D. A. Kulpa and N. Chomont, *J. Virus Erad.*, 2015, **1**, 59-66.
2. T.-W. Chun, S. Moir and A. S. Fauci, *Nat. Immunol.*, 2015, **16**, 584-589.
3. C. Schwartz, S. Bouchat, C. Marban, V. Gautier, C. Van Lint, O. Rohr and V. Le Douce, *Biochem. Pharmacol.*, 2017, **146**, 10-22.
4. A. Sosnik, *Nanomedicine*, 2010, **5**, 833-837.
5. R. Rose, D. J. Nolan, E. Maidji, C. A. Stoddart, E. J. Singer, S. L. Lamers and M. S. McGrath, *AIDS Res. Hum. Retroviruses*, 2017.
6. B. K. Titanji, D. Pillay and C. Jolly, *J. Gen. Virol.*, 2017, **98**, 821-834.
7. A. F. Capetti, M. Micale, L. Carenzi, F. Niero, S. Landonio, S. Vimercati, G. Dedivitiis and G. Rizzardini, *Medicine (Baltimore)*, 2017, **96**, e5728.
8. R. R. Adhikary, P. More and R. Banerjee, *Nanoscale*, 2015, **7**, 7520-7534.
9. J. Lisziewicz and E. R. Toke, *Nanomedicine*, 2013, **9**, 28-38.
10. S. D. Mahajan, R. Aalinkeel, W.-C. Law, J. L. Reynolds, B. B. Nair, D. E. Sykes, K.-T. Yong, I. Roy, P. N. Prasad and S. A. Schwartz, *Int. J. Nanomedicine*, 2012, **7**, 5301-5314.
11. J. das Neves, M. M. Amiji, M. F. Bahia and B. Sarmento, *Adv. Drug. Deliv. Rev.*, 2010, **62**, 458-477.
12. J. das Neves, R. Nunes, F. Rodrigues and B. Sarmento, *Adv. Drug Deliv. Rev.*, 2016, **103**, 57-75.
13. J. das Neves, B. Sarmento and A. Sosnik, *Adv. Drug Deliv. Rev.*, 2016, **103**, 1-4.
14. J. D. Siliciano, J. Kajdas, D. Finzi, T. C. Quinn, K. Chadwick, J. B. Margolick, C. Kovacs, S. J. Gange and R. F. Siliciano, *Nat. Med.*, 2003, **9**, 727-728.
15. P. Kumar, Y. S. Lakshmi and A. K. Kondapi, *Pharm. Res.*, 2017, **34**, 257-268.
16. W. Li, F. Yu, Q. Wang, Q. Qi, S. Su, L. Xie, L. Lu and S. Jiang, *Aids*, 2016, **30**, 827-838.
17. T. Chaowanachan, E. Krogstad, C. Ball and K. A. Woodrow, *PLoS One*, 2013, **8**, e61416.

18. Y. Jiang, S. Cao, D. K. Bright, A. M. Bever, A. K. Blakney, I. T. Suydam and K. A. Woodrow, *Mol. Pharm.*, 2015, **12**, 4363-4374.
19. A. Dalpiaz, L. Ferraro, D. Perrone, E. Leo, V. Iannuccelli, B. Pavan, G. Paganetto, S. Beggiato and S. Scalia, *Mol. Pharm.*, 2014, **11**, 1550-1561.
20. J. P. Freeling, J. Koehn, C. Shu, J. Sun and R. J. Y. Ho, *Aids*, 2014, **28**, 2625-2627.
21. J. Della Rocca, D. Liu and W. Lin, *Acc. Chem. Res.*, 2011, **44**, 957-968.
22. P. Horcajada, R. Gref, T. Baati, P. K. Allan, G. Maurin, P. Couvreur, G. Ferey, R. E. Morris and C. Serre, *Chem. Rev.*, 2012, **112**, 1232-1268.
23. V. Agostoni, T. Chalati, P. Horcajada, H. Willaime, R. Anand, N. Semiramoth, T. Baati, S. Hall, G. Maurin, H. Chacun, K. Bouchemal, C. Martineau, F. Taulelle, P. Couvreur, C. Rogez-Kreuz, P. Clayette, S. Monti, C. Serre and R. Gref, *Adv. Healthcare Mat.*, 2013, **2**, 1630-1637.
24. M. T. Marcos-Almaraz, R. Gref, V. Agostoni, C. Kreuz, P. Clayette, C. Serre, P. Couvreur and P. Horcajada, *J. Mater. Chem. B*, 2017, **5**, 8563-8569.
25. P. Horcajada, T. Chalati, C. Serre, B. Gillet, C. Sebrie, T. Baati, J. F. Eubank, D. Heurtaux, P. Clayette, C. Kreuz, J. S. Chang, Y. K. Hwang, V. Marsaud, P. N. Bories, L. Cynober, S. Gil, G. Ferey, P. Couvreur and R. Gref, *Nat. Mater.*, 2010, **9**, 172-178.
26. M. Giardiello, N. J. Liptrott, T. O. McDonald, D. Moss, M. Siccardi, P. Martin, D. Smith, R. Gurjar, S. P. Rannard and A. Owen, *Nat. Commun.*, 2016, **7**.
27. T. O. McDonald, M. Giardiello, P. Martin, M. Siccardi, N. J. Liptrott, D. Smith, P. Roberts, P. Curley, A. Schipani, S. H. Khoo, J. Long, A. J. Foster, S. P. Rannard and A. Owen, *Adv. Healthcare Mat.*, 2014, **3**, 400-411.
28. W. J. Rieter, K. M. Pott, K. M. L. Taylor and W. B. Lin, *J. Am. Chem. Soc.*, 2008, **130**, 11584-+.
29. L. Xing, Y. Y. Cao and S. A. Che, *Chem. Commun.*, 2012, **48**, 5995-5997.
30. R. C. Huxford, K. E. deKrafft, W. S. Boyle, D. M. Liu and W. B. Lin, *Chem. Sci.*, 2012, **3**, 198-204.
31. N. N. Adarsh, C. Frias, T. M. P. Lohidakshan, J. Lorenzo, F. Novio, J. Garcia-Pardo and D. Ruiz-Molina, *Chem. Eng. J.*, 2018, **340**, 94-102.
32. F. Novio, J. Lorenzo, F. Nador, K. Wnuk and D. Ruiz-Molina, *Chem. Eur. J.*, 2014, **20**, 15443-15450.
33. L. Xing, H. Q. Zheng, Y. Y. Cao and S. A. Che, *Adv. Mater.*, 2012, **24**, 6433-6437.
34. I. Imaz, M. Rubio-Martinez, L. Garcia-Fernandez, F. Garcia, D. Ruiz-Molina, J. Hernando, V. Puntes and D. Maspoch, *Chem. Commun.*, 2010, **46**, 4737-4739.
35. C. B. He, D. M. Liu and W. B. Lin, *Chem. Rev.*, 2015, **115**, 11079-11108.
36. R. C. Huxford-Phillips, S. R. Russell, D. M. Liu and W. B. Lin, *Rsc Adv.*, 2013, **3**, 14438-14443.
37. D. Liu, C. Poon, K. Lu, C. He and W. Lin, *Nat. Commun.*, 2014, **5**, 4182.
38. C. Poon, C. He, D. Liu, K. Lu and W. Lin, *J. Control Release*, 2015, **201**, 90-99.
39. L. Amorin-Ferre, F. Busque, J. L. Bourdelande, D. Ruiz-Molina, J. Hernando and F. Novio, *Chem. Eur. J.*, 2013, **19**, 17508-17516.
40. F. Nador, F. Novio and D. Ruiz-Molina, *Chem. Commun. (Camb)*, 2014, **50**, 14570-14572.
41. M. R. Blum, S. H. Liao, S. S. Good and P. de Miranda, *Am. J. Med.*, 1988, **85**, 189-194.
42. A. Khandazhinskaya, E. Matyugina and E. Shirokova, *Expert Opin. Drug Metab. Toxicol.*, 2010, **6**, 701-714.
43. S. R. Ribone, E. M. Schenfeld, M. Madrid, A. B. Pierini and M. A. Quevedo, *New J. Chem.*, 2016, **40**, 2383-2392.
44. D. H. Jo, Y.-M. Chiou and L. Jr Que, *Inorg. Chem.,* 2001, **40**, 3181-3190.
45. T. L. Moore, L. Rodriguez-Lorenzo, V. Hirsch, S. Balog, D. Urban, C. Jud, B. Rothen-Rutishauser, M. Lattuada and A. Petri-Fink, *Chem. Soc. Rev.*, 2015, **44**, 6287-6305.
46. P. Aggarwal, J. B. Hall, C. B. McLeland, M. A. Dobrovolskaia and S. E. McNeil, *Adv. Drug Deliver. Rev.*, 2009, **61**, 428-437.
47. M. G. Anhorn, H. C. Mahler and K. Langer, *Int. J. Pharm.*, 2008, **363**, 162-169.
48. D. T. Chiu and P. H. Duesberg, *Genetica*, 1995, **95**, 103-109.
49. M. Borges, S. Yu, A. Laromaine, A. Roig, S. Suarez-Garcıa, J. Lorenzo, D. Ruiz-Molina and F. Novio, *RSC Adv.*, 2015, **5**, 86779–86783.
50. M. Tsiang, G. S. Jones, J. Goldsmith, A. Mulato, D. Hansen, E. Kan, L. Tsai, R. A. Bam, G. Stepan, K. M. Stray, A. Niedziela-Majka, S. R. Yant, H. Yu, G. Kukolj, T. Cihlar, S. E. Lazerwith, K. L. White and H. Jin, *Antimicrob. Agents Chemother.*, 2016, **60**, 7086-7097.
51. L. M. Bedoya, M. Beltran, P. Obregon-Calderon, J. Garcia-Perez, H. E. de la Torre, N. Gonzalez, M. Perez-Olmeda, D. Aunon, L. Capa, E. Gomez-Acebo and J. Alcami, *Aids*, 2016, **30**, 2767-2776.
52. R. M. Oguariri, L. Dai, J. W. Adelsberger, A. Rupert, R. Stevens, J. Yang, D. Huang, R. A. Lempicki, M. Zhou, M. W. Baseler, H. C. Lane and T. Imamichi, *J. Biolog. Chem.*, 2013, **288**, 17812-17822.
53. R. M. Mainardes, M. P. D. Gremiao, I. L. Brunetti, L. M. Da Fonseca and N. M. Khalil, *J. Pharm. Sci-Us*, 2009, **98**, 257-267.
54. S. Mandal, Y. Zhou, A. Shibata and C. J. Destache, *Aip. Adv.*, 2015, **5**.
55. A. S. Nowacek, R. L. Miller, J. McMillan, G. Kanmogne, M. Kanmogne, R. L. Mosley, Z. Ma, S. Graham, M. Chaubal, J. Werling, B. Rabinow, H. Dou and H. E. Gendelman, *Nanomedicine (Lond)*, 2009, **4**, 903-917.
56. A. Beduneau, Z. Ma, C. B. Grotepas, A. Kabanov, B. E. Rabinow, N. Gong, R. L. Mosley, H. Dou, M. D. Boska and H. E. Gendelman, *PLoS One*, 2009, **4**, e4343.
57. A. Vonarbourg, C. Passirani, P. Saulnier, P. Simard, J. C. Leroux and J. P. Benoit, *J. Biomed. Mat. Res. Part A*, 2006, **78**, 620-628.
58. Y. Tabata and Y. Ikada, *Biomaterials*, 1988, **9**, 356-362.
59. T. P. Zimmerman, W. B. Mahony and K. L. Prus, *J. Biolog Chem.*, 1987, **262**, 5748-5754.
60. E. Errasti-Murugarren and M. Pastor-Anglada, *Pharmacogenomics*, 2010, **11**, 809-841.
61. B. Sillman, A. N. Bade, P. K. Dash, B. Bhargavan, T. Kocher, S. Mathews, H. Su, G. D. Kanmogne, L. Y. Poluektova, S. Gorantla, J. McMillan, N. Gautam, Y. Alnouti, B. Edagwa and H. E. Gendelman, *Nat. Commun.*, 2018, **9**, 443.